Biomaterials 35 (2014) 6236–6247

Contents lists available at ScienceDirect

Biomaterials

journal homepage: www.elsevier.com/locate/biomaterials

The role of physiological mechanical cues on mesenchymal stem cell differentiation in an airway tract-like dense collagen–silk fibroin construct

Chiara E. Ghezzi [a], Benedetto Marelli [a], Ilaria Donelli [b], Antonio Alessandrino [b], Giuliano Freddi [b], Showan N. Nazhat [a,*]

[a] Department of Mining and Materials Engineering, McGill University, Montreal, Quebec, Canada H3A 2B2
[b] Innovhub – Stazioni Sperimentali per l'Industria, Div. Stazione Sperimentale per la Seta, Milan, Italy

ARTICLE INFO

Article history:
Received 17 March 2014
Accepted 14 April 2014
Available online 10 May 2014

Keywords:
Dense collagen gel
Silk fibroin
Trachea
Airway smooth muscle cells
Cartilage

ABSTRACT

Airway tracts serve as a conduit of transport in the respiratory system. Architecturally, these are composed of cartilage rings that offer flexibility and prevent collapse during normal breathing. To this end, the successful regeneration of an airway tract requires the presence of differentiated chondrocytes and airway smooth muscle cells. This study investigated the role of physiological dynamic mechanical stimulation, *in vitro*, on the differentiation of mesenchymal stem cells (MSCs), three-dimensionally seeded within a tubular dense collagen matrix construct-reinforced with rings of electrospun silk fibroin mat (TDC–SFC). In particular, the role of either shear stress supplied by laminar fluid flow or cyclic shear stress in combination with circumferential strain, provided by pulsatile flow, on the chondrogenic differentiation, and contractile lineage of MSCs, and their effects on TDC–SFC morphology and mechanical properties were analysed. Chondrogenic differentiation of MSCs was observed in the presence of chondrogenic supplements under both static and laminar flow cultures. In contrast, physiological pulsatile flow resulted in preferential cellular orientation within TDC–SFC, as dictated by dynamic circumferential strain, and induced MSC contractile phenotype expression. In addition, pulsatile flow decreased MSC-mediated collagen matrix remodelling and increased construct circumferential strength. Therefore, TDC–SFC demonstrated the central role of a matrix in the delivery of mechanical stimuli over chemical factors, by providing an *in vitro* niche to control MSC differentiation, alignment and its capacity to remodel the matrix.

1. Introduction

Tissue engineering aims to replace damaged or diseased tissues by creating functional neo-tissues *in vitro* through the use of committed cells and dedicated scaffolds. In addition to providing clinical therapies for replacing organs and hierarchical tissues, engineered organ and tissue replica have also been developed to create *in vitro* tissue models [1]. These models are designed to study complex physiological and pathological mechanisms *in vitro*; supporting the development of therapies to prevent or cure underlying diseases [2]. In the case of tubular tissues, these constructs also present an increased level of complexity in terms of geometry and architecture, together with a mixed cell population, and constant cyclic mechanical stimulation that modulate cellular responses and ultimately the functionality of the tissues. In particular, airway tracts, which represent the conduit of transport in the respiratory system, are affected by diverse medical conditions ranging from neoplasms and trauma injuries to inflammatory and degenerative diseases (*e.g.* asthma and cystic fibrosis), which require functional three-dimensional (3D) airway tissue substitutes and models to be used in clinical settings [3].

Native airway tracts should be flexible and compliant to accommodate the respiratory movements and structurally stable to prevent collapse during normal breathing. Therefore, airway tissue is reinforced by cartilage rings to maintain conduit flexibility without structural instability during inspiration [4]. Several 3D tissue-engineered airways have been proposed, which are mainly based on biodegradable synthetic polymers and in combination

* Corresponding author. Department of Mining and Materials Engineering, McGill University, 3610 University Street, Montreal, Quebec, Canada H3A 2B2.
Tel.: +1 514 398 5524; fax: +1 514 398 4492.
E-mail address: showan.nazhat@mcgill.ca (S.N. Nazhat).

http://dx.doi.org/10.1016/j.biomaterials.2014.04.040
0142-9612/

with helical elastomeric templates to mimic tracheal geometrical features [5–7]. However, the use of non-biologically derived constructs has been shown to illicit an acute inflammatory reaction and discourage cell invasion, growth, and organization [8]. Therefore, natural polymers (*e.g.* type I collagen gels and sponges) have been implemented in combination with synthetic polymers to increase the biocompatibility of the engineered airway tissues [9–12]. Yet, the inherent complexity of processing composite, multilayered, and hybrid materials limits the translation of these scaffolds into clinical use [3]. In contrast, tissue-engineered airway constructs based purely on natural polymers have not been largely investigated, due to the limited mechanical properties of naturally derived hydrogels, *e.g.* hyaluronic acid, type I collagen and fibrin [13] and, although silk fibroin displays high strength and stiffness, it has only been used as a coating in rabbit tracheal defect reconstruction [14].

Along with a construct, a suitable cell source should be readily available in large volumes to be effectively used in tissue engineering approaches. In this view, mesenchymal stem cells (MSCs) represent a potential candidate for generating mesenchyme cells in bone, vascular, cartilage, and nerve tissue substitutes and models. In addition, since MSCs have the ability to differentiate into a variety of cell types; including chondrocytes and smooth muscle cells (SMCs) [15], they can also be considered for the regeneration of the airway tract. MSC differentiation has been shown to be affected by soluble factors, substrate stiffness and topography, as well as dynamic mechanical stimulation, such as shear stress and cyclic strain [16–19]. In particular, it has recently been demonstrated that the *in vitro* mechanotransduction of external mechanical stimulation regulates MSC growth [20], cytoskeleton organization [21], and its osteogenic, chondrogenic and contractile phenotypes [21–23]. Optimized and balanced culture profiles have been shown to significantly improve *in vitro* engineered tissues (*e.g.* ligament), where sequential biochemical and mechanical stimulations have been alternated [24]. However, systematic studies focused on segregating the effects of chemical and mechanical cues on MSC differentiation when seeded in a 3D physiologically relevant construct has not been extensively reported.

To this end, this study investigated the role of physiological mechanical stimulation, *in vitro*, on the differentiation of MSCs, seeded within an airway tract-like electrospun silk fibroin ring-reinforced tubular dense collagen construct (TDC–SFC). The effect of shear stress supplied by laminar flow of complete medium with or without growth factor supplements (chondrogenic medium) or shear stress in combination with cyclic circumferential strain, provided by pulsatile flow, on the chondrogenic differentiation, and contractile lineage of MSCs, orientation, and their effects on TDC–SFC morphology and mechanical properties were analysed.

2. Materials and methods

2.1. MSC culture

MSCs, extracted from bone marrow isolated from C57BL/6 mice at < 8 weeks of gestation through mechanical and enzymatic digestion were purchased from Invitrogen (Carlsbad, CA, USA). According to the manufacturer's instructions, C57BL/6 MSCs below passage 10 express a flow-cytometry cell-surface protein profile positive for CD29, CD34, and Sca-1 (>70%), and negative for CD117 (<5%). The cells were expanded and cultured in complete growth medium, prepared from Dulbecco's Modified Eagle Medium F-12 (DMEM/F-12, Gibco®, Invitrogen, Carlsbad, CA, USA) with GlutaMAX™-I containing 10% MSC-Qualified Foetal Bovine Serum (FBS, Gibco®, Invitrogen, Carlsbad, CA, USA) and 5 μg/ml Gentamicin (Gibco®, Invitrogen, Carlsbad, CA, USA). MSCs were expanded up to passage 8 to prevent dedifferentiation.

2.2. Preparation of electrospun silk fibroin mat

Bombyx mori cocoons were purchased from the Unità di ricerca di apicultura e bachicoltura (CRA-API), Sezione Bachicoltura, Padova, Italy. Sericin extraction was carried out by autoclaving at 120 °C for 15 min and rinsing in deionized water until complete removal of the globular protein [25]. The resulting SF fibres were neutralized and dissolved in a saturated lithium bromide solution (Sigma–Aldrich, Italy) at 60 °C. The 10% (w/v) solution was then dialysed against deionized water with D9402 dialysis tubing cellulose membrane (Sigma–Aldrich, Italy), obtaining a final SF aqueous solution concentration of ~2% (w/v). SF films were prepared by solvent casting at room temperature.

As previously described [26], electrospun SF mats were prepared by dissolving SF films in formic acid (98 vol.%, Sigma–Aldrich, Italy) at room temperature under gentle stirring. SF solution (final concentration of 7.5%) was then transferred into a 50 ml syringe and electrospun using an *ad-hoc* electrospinning apparatus [27] using a flow rate of 1.1 ml/h, an electric field of 24 kV, and an electrode distance of 10 cm for a deposition time of 2 h [27]. The SF mats were then treated in methanol for 15 min to increase SF crystallinity [28].

2.3. Preparation of MSC-seeded TDC–SFCs

A tubular construct was prepared using a previously established methodology based on dense collagen [29], which was reinforced with electrospun SF insertion in order to mimic the natural airway architecture and increase the structural and mechanical properties (Fig. 1A). SF mats were cut into 3 mm-wide strips with a surgical scalpel, and then sterilized by immersion in 70% ethanol overnight and subsequently rinsed in sterile water [30] (Fig. 1Ai). Neutralized collagen solution was prepared by adding 12 ml of solubilized bovine dermis type I collagen solution (4.8 mg/ml in acidic solution, Collagen Solutions LLC, San Jose, CA, USA) to 3 ml of 10× DMEM (Sigma–Aldrich, Canada), and aliquots of 5 M NaOH (Sigma–Aldrich, Canada). MSCs were incorporated into the neutralized collagen solution at a cell density of 2.11×10^5 cells/ml (Fig. 1Aii). The cellular collagen solution was initially poured into the bottom part of vertically stacking sub-mould ($45 \times 50 \times 7$ mm^3), designed to stabilize four SF electrospun strips inserted in the middle of collagen solution equidistant from the mould extremities (Fig. 1Aiii), as previously described with a rectangular SF mat in a planar geometry [26]. Post collagen gelation at 37 °C for 30 min, the highly hydrated collagen gel–SF hybrid (Fig. 1Aiv) was transferred onto blotting paper, supported by stainless steel mesh. Plastic compression was applied with an unconfined compressive stress equivalent to 1 kPa for 5 min, resulting in the multilayered hybrid assembly composed of two DC sheets reinforced with unidirectionally aligned electrospun SF strips (Fig. 1Av). TDC–SFC was generated by rolling the DC–SF–DC hybrid assembly along the long axis of a cylindrical polytetrafluoroethylene mandrel (3.4 mm diameter) into three concentric layers of approximately 550 μm wall thickness (Fig. 1Avi, B) [29].

2.4. Dynamic culturing

Acellular and MSC-seeded TDC–SFCs were dynamically stimulated via either pulsatile or laminar flow and compared to static culturing for 7 days (Table 1). In particular, the samples investigated were named as follows: acellular as made sample (A_{made}), acellular sample cultured in static condition (A_{static}), acellular sample cultured under pulsatile flow (A_{pulse}), cell-seeded sample cultured in static condition (C_{static}), cell-seeded sample cultured under laminar flow ($C_{laminar}$), and cell-seeded sample cultured under pulsatile flow (C_{pulse}). Immediately after preparation, TDC–SFCs were gently removed from the cylindrical mandrel, inserted on both sides of plastic barbed fittings attached to the anchor shafts of the bioreactor chamber and securely tightened with 4-0 suture threads (Perma-Hand, Ethicon Inc., USA) to prevent fluid leakage, as previously reported [31]. The assembly was placed in an incubator (Forma Environmental Chamber 3920, Thermo Scientific, Canada) for precise environmental control (*i.e.* 37 °C and CO_2 at 5%). Pulsatile flow (C_{pulse}) was generated by an ElectroForce® Biodynamic Test Instrument 5160 (Bose Corp., USA) equipped in vascular configuration. A gear pump (Micropump Inc. of Index Corporation, USA) was used to supply a steady flow (75 ml/min) in series with a pulsatile manifold to generate a waveform of 1 Hz frequency and 25 ml/min of dynamic flow amplitude. The pulsatile flow parameters resulted in transmural tracheal pressure oscillations of 20/30 cmH_2O and <5% circumferential strain measured with an intraluminal Mikro-Tip® Catheter Pressure Transducer (Millar Instruments, Inc., USA). For comparison, TDC–SFCs were also cultured under laminar flow ($C_{laminar}$) of steady flow of 75 ml/min. In all tests, an additional TDC–SFC was also cultured in the chamber freely floating as static control (C_{static}) and the culturing medium (300 ml) was replaced at day 4. MSC-seeded TDC–SFCs were cultured for 7 days in either chondrogenic (CD) or control growth (ND) media for comparison. CD medium consisted of complete growth medium further supplemented with 200 ng/ml of insulin-like growth factor-I (IGF-I, R&D Systems, Inc., MN, USA) and 1 ng/ml of transforming growth factor-beta (TGF-beta, R&D Systems, Inc., MN, USA).

Mean wall shear stress, τ_{mean} (dyn/cm^2), was calculated using the Hagen–Poiseuille equation [32] as $\tau_{mean} = 4\mu Q/\pi R_0^3$, where μ is the dynamic viscosity of the culture medium with 10% FBS (1 cP [33]), Q is the volumetric flow rate (ml/min), and R_0 is the TDC–SFC internal radius. The mean shear stress applied during the cycle was calculated as $\tau_{mean} = 3.2 \pm 1$ dyne/cm^2, in the range of luminal shear stress generated by airflow at rest breathing (0.5–3 dyne/cm^2) [34].

2.5. MSC viability and distribution

MSC viability within C_{pulse} and C_{static} was assessed at day 7 in CD. DC–SF–DC ring-shaped specimens (5 mm in length) were incubated for 60 min in complete

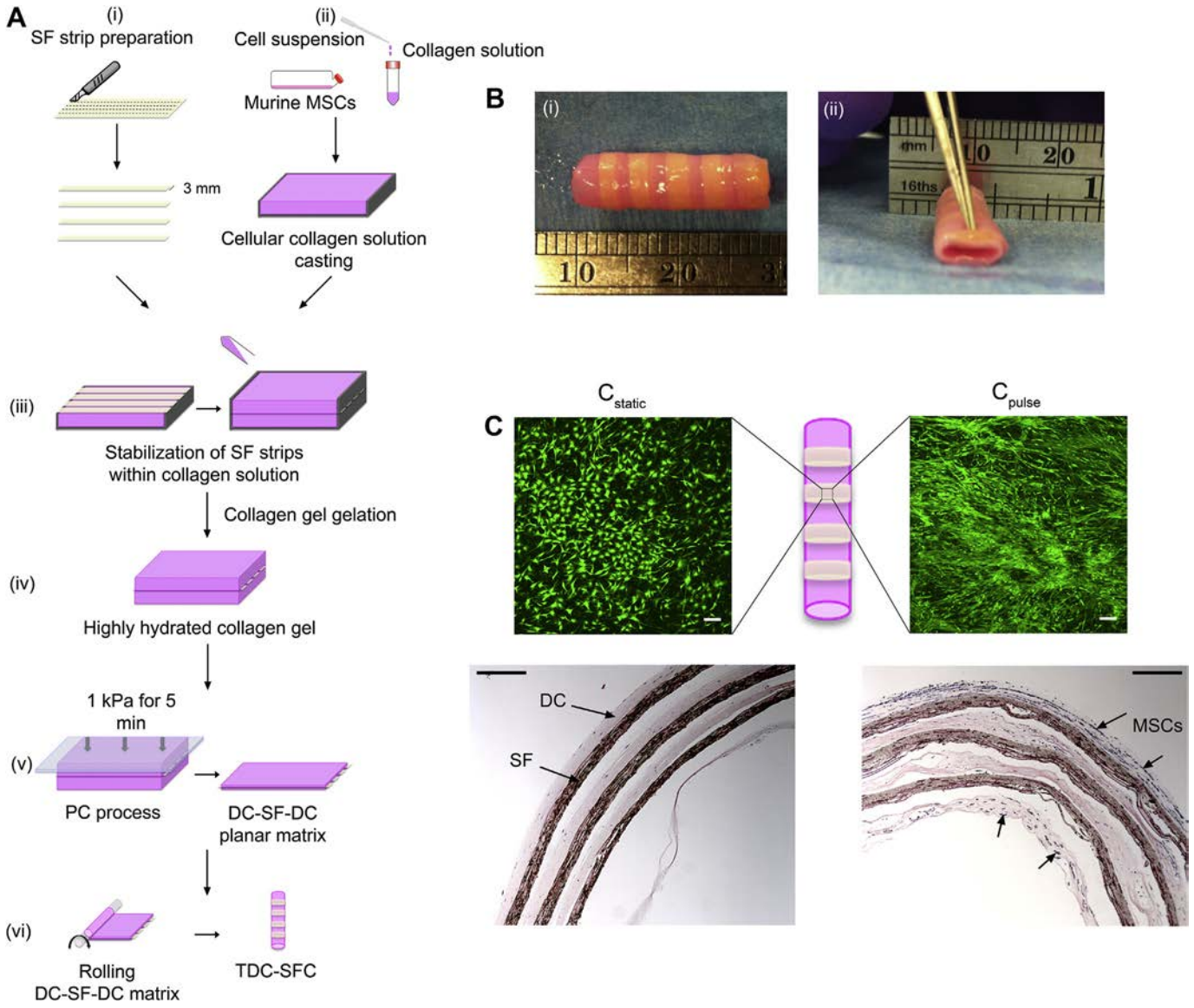

Fig. 1. Schematic of MSC-seeded TDC-SFC hybrid preparation and culture. A. (i) Electrospun SF mat, used to reinforce DC constructs, was divided into 3 mm-wide strips with a surgical scalpel. (ii) MSCs were added to the neutralized collagen solution. The MSC incorporated collagen solution was initially cast in the bottom part of vertically stacking two sub-moulds. (iii) Four equidistant electrospun SF strips were stabilized in the middle of collagen solution. (iv) Post collagen gelation at 37 °C for 30 min, the resultant highly hydrated collagen gel–SF hybrid was transferred onto blotting paper, supported by stainless steel mesh. (v) PC was applied using 1 kPa for 5 min to generate MSC-seeded hybrid assembly comprised of DC sheets reinforced with electrospun SF strips. (vi) TDC–SFCs were generated by rolling the hybrid sheets along their long axis and around a cylindrical polytetrafluoroethylene mandrel (3.4 mm diameter) to generate three concentric layers of approximately 550-μm total wall thickness. B. Macroscopic view of TDC–SFC hybrid. (i) Close-up image of TDC–SFC. (ii) Structural resistance of TDC–SFC upon localized compressive load. C. MSC viability and distribution. Evaluation of the viability of 3D seeded MSCs within the TDC–SFC at day 7 in CD for C_{static} and C_{pulse}. Longitudinal CLSM maximum intensity projection images of calcein-AM labelled and ethidium homodimer-1 binding MSCs within TDC–SFCs display viable cells throughout the entire wall (top panel). Scale bar = 200 μm. Representative images of H&E stained histological sections of C_{static} and C_{pulse} at day 7 in CD (bottom panel). MSCs were homogenously distributed both radially and circumferentially within the TDC–SFC walls. Scale bar = 500 μm.

medium with 1 μM calcein-AM and 2 μM ethidium homodimer-1 (Live/Dead® assay, Invitrogen, USA), and positive staining evaluated with a confocal laser scanning microscope (CLSM, LSM 5, Carl Zeiss, Germany). Images were acquired with argon laser excitation (488 nm) and HeNe633 laser excitation (543 nm) with a 10× objective. Z-stacks were obtained from 15 μm slices through the entire TDC–SFC wall thickness in 3 different regions of the ring. Representative images were reconstructed as maximum intensity projections using ImageJ software (Rasband, W.S., ImageJ, US, National Institute of Health, Bethesda, USA, http://rsb.info.nih.gov/ij/, 1997–2010).

Haematoxylin and eosin (H&E) stained histological sections were analysed with a light microscopy (4×, Leica DM500) to evaluate MSC distribution within C_{static} and C_{pulse} at day 7. Ring-shaped specimens were equilibrated in phosphate buffered saline (PBS) and fixed in 10% neutral buffered formalin (Protocol, Fisher Scientific) overnight. TDC–SFC sections were dehydrated through a series of graded ethanol solutions, embedded in paraffin and cut in transverse sections of 5 mm thickness. Histological sections were then deparaffinized, rehydrated through a series of graded ethanol, and stained with H&E.

2.6. MSC alignment

Scanning electron microscopy (SEM), and CLSM, to image F-actin staining, were used to evaluate the effect of pulsatile and laminar flows applied for 7 days on MSC distribution, and alignment within TDC–SFCs.

MSC morphology and alignment on the internal and external surfaces of C_{static}, $C_{laminar}$ and C_{pulse} were analysed through SEM. The constructs were harvested after 7 days and cut into 5 mm sections, washed in PBS and then fixed in 4% para-formaldehyde–0.1 M sodium cacodylate solution overnight at 4 °C. After washing with deionized distilled water, samples were dehydrated at 4 °C through sequential exposure to a gradient of ethanol, and then processed with a critical point dryer (Ladd Research Industries, USA), sputter coated with Au/Pd (Hummer VI Sputter

Table 1
TDC–SFC sample description.

Material description	ASMC seeded	Stimulation	Time in culture [day]
A_{made}		None	0
A_{static}		None	7
A_{pulse}		Pulsatile flow	7
C_{static}	X	None	7
$C_{laminar}$	X	Laminar flow	7
C_{pulse}	X	Pulsatile flow	7

Coater, Ladd Research Industries, USA) and analysed by SEM (S-4700 Field Emission-STEM, Hitachi, Japan) at 2 kV and 10 μA.

MSC alignment was also characterized through CLSM imaging of F-actin filaments distribution in relation to direction of the fluid flow and the circumferential strain. At day 7 in culture, specimens were cut into 5 mm segments, washed in PBS and fixed in 3.7% methanol-free formaldehyde (Polyscience Inc., USA) for 10 min at room temperature. Afterwards the specimens were washed in PBS, permeabilized in 99% acetone (Sigma Aldrich, Canada) at −20 °C for 5 min and rewashed in PBS. To reduce nonspecific background staining, the samples were pre-incubated with PBS containing 1% bovine serum albumin (BSA, Sigma Aldrich, Canada) for 20 min. The TDC–SFC segments were incubated with Alexa Fluor® 633 Phalloidin (Molecular Probes™, Invitrogen, USA) at 1:40 for 20 min at room temperature. Images were acquired using argon laser excitation (633 nm) with a 10× objective. Z-stacks were obtained through approximately 150-μm thickness of the internal and external TDC–SFC wall using 10 μm slices in 5 different regions. Afterwards, z-stacks were assembled into maximum intensity projection reconstructions.

2.7. MSC differentiation

Histological staining with Safranin-O and anti-collagen II primary antibody, and ring-shaped specimen staining with α-smooth muscle actin (αSMA) together with real-time quantitative Reverse Transcription-Polymerase Chain Reaction (RT-qPCR) were used to assess chondrogenic and contractile differentiation of MSCs, in response to 7-day pulsatile and laminar flow stimulation in comparison to static culture in either CD or ND.

Histological sections, prepared as described above, were deparaffinized, stained with Safranin-O solution, and then observed with a light microscope using a 4× objective. Collagen type II deposition was investigated using CLSM; histological sections were deparaffinized, rehydrated through a series of graded ethanol, incubate in retrieval solution overnight, and then incubated overnight with the primary antibody, anti-collagen II (1:500; ab3092, Abcam). After washing in Tris buffer saline, sections were incubated for 1 h in secondary antibody solution, Goat F(ab′)2 polyclonal Secondary Antibody to Mouse IgG (1:500; ab98758, Abcam). CLSM images were acquired with HeNe633 laser excitation (543 nm) with a 10× objective.

MSC contractile differentiation was observed through CLSM imaging of αSMA distribution. Ring-shaped specimens were prepared as described above for F-actin staining and incubated with FITC monoclonal anti-α-SMA (Sigma Aldrich, Canada) at a working dilution of 1:200 for 1 h at 37 °C. Images were acquired using argon laser excitation (488 nm) with a 10× objective. Z-stacks were obtained through approximately 150-μm thickness of the internal and external TDC–SFC walls using 10 μm slices in 5 different regions, and reconstructed into maximum intensity projection.

Expression levels of various chondrogenic and contractile genes to investigate MSC differentiation state and selected matrix metalloproteinase's (MMPs) activities were assessed within $C_{laminar}$ and C_{pulse} constructs in comparison to C_{static} in CD and ND by quantitative RT-PCR in 3 separate independent experiments. At day 7, total RNA was extracted with TRIzol ® (Invitrogen, Carlsbad, CA, USA) following the manufacturer's instructions. After RNA separation, nucleic acid concentration and integrity were determined with an Eppendorf BioPhotometer Plus (Eppendorf, Hamburg, Germany). 250 ng of total RNA was mixed with 0.25 ng of random hexamers (Invitrogen, Carlsbad, CA, USA) and reverse-transcribed into complementary DNA (cDNA) with 200 U of Superscript Reverse Transcriptase II (Invitrogen, Carlsbad, California) and RNasin (Promega). Quantitative RT-PCR was performed with an ABI Prism 7900 HT 139 (Applied Biosystems). Each PCR reaction contained 9 μl of cDNA, 0.5 μl of both forward and reverse primers (10 μM), and 10 μl of SYBR Green (Applied Biosystems). The cycling conditions were: 50 °C for 2 min, initial denaturation at 95 °C for 10 min, and 45 cycles of 15 s at 95 °C and 1 min at 60 °C. Relative quantification of target gene expression was achieved first normalizing to an endogenous reference gene (housekeeping gene GAPDH) to correct different amounts of input RNA, and then relating the expression of the target genes to a reference sample (C_{static}) cultured in the same condition using the $-2\Delta\Delta$Ct method [35]. Sequences of primers and amplicon size are listed in Table 2.

2.8. Morphological characterization

The influence of pulsatile flow and MSC-mediated remodelling on TDC–SFC structural and morphological properties were investigated through micro-computed tomography (microCT), and Sirius Red (SR) stained histological sections.

Table 2
Primer sequences and amplicon size for RT-qPCR.

Gene	Primers	Size
GAPDH	5′-ACCACAGTCCATGCCATCAC-3′ 5′-TCCACCACCCTGTTGCTGTA-3′	452
α1(II) Collagen (Col2a1)	5′-GCGGTGAGCCATGATCCGCC-3′ 5′-GCGACTTACGGGCATCCT-3′	104
Aggrecan (Agg)	5′-GAAATGACAACCCCAAGCAC-3′ 5′-TCTCCGCTGATTTCAGTCCT-3′	188
Actin alpha 2 (Acta2)	5′-GGCTGTTTTCCCATCCATCG-3′ 5′-CCCATTCCAACCATTACTCCCTG-3′	60
Calponin 1 (Calp1)	5′-ACCAACCATACACAAGTTCAGTCC-3′ 5′-CCAATGATGTTCCTGCCTTCTCTC-3′	152
Myosin heavy chain (MHC)	5′-AGAAATGGACGCTCGGGACTC-3′ 5′-TCTGTGACTTGAGAACGAATGGAC-3′	153
Desmin (Des)	5′-GTGAAGATGGCCTTGGATGT-3′ 5′-GTAGCCTCGCTGACAACCTC-3′	209
Matrix metalloproteinase 1a (MMP1a)	5′-GTCTTTGAGGAGGAAGGCGATATT-3′ 5′-AGTTAGGTCCATCAAATGGGTTGTT-3′	82
Matrix metalloproteinase 2 (MMP2)	5′-AACTACGATGATGACCGGAAGTG-3′ 5′-TGGCATGGCCGAACTCA-3′	88
Matrix metalloproteinase 3 (MMP3)	5′-GGAAATCAGTTCTGGGCTATACGA-3′ 5′-TAGAAATGGCAGCATCGATCTTC-3′	112
Matrix metalloproteinase 13 (MMP13)	5′-GGGCTCTGAATGGTTATGACATTC-3′ 5′-AGCGCTCAGTCTCTTCACCTCTT-3′	89
Tissue inhibitor of metalloproteinase 1 (Timp1)	5′-GTGGGAAATGCCGCAGATATC-3′ 5′-GACCTGATCCGTCCACAAAC-3′	300

MicroCT analysis was performed on wet TDC–SFCs with a SkyScan 1172 (SkyScan, Belgium) to characterize the stability of the hybrid three-layered structure of C_{static}, $C_{laminar}$, and C_{pulse} after 7 days in CD culture. Samples were analysed through a 360° flat-field corrected scan at 68 kV and 173 μA, with a step size of 0.68°, a resolution of 11.5 μm, a medium camera pixel, and no filter. The volumetric reconstruction (NRecon software, SkyScan) was set with a beam hardening correction of 10, a ring artifact correction of 20 and an "auto" misalignment correction. Two-dimensional analysis (software CTAn, SkyScan) was carried out using a grayscale intensity range of 20–255 (8 bit images) to remove background noise. Hounsfield unit (HU) was used to measure construct bulk density generated through standard calibration [29].

Collagen organization was investigated through SR staining of tissue sections, which enhances the birefringency of organized collagen under polarized light [36]. SR stained collagen fibrils act as a polarization filter due to their highly organized structure. The sections were interposed between two perpendicularly oriented polarization filters and observed via light microscopy (Leica DM500) equipped with polarized light optics.

2.9. Mechanical characterization

Acellular and MSC-seeded TDC–SFC mechanical properties were investigated at day 7 through circumferential tensile testing (CTT), and calculation of estimated burst pressure. TDC–SFC compliance was measured on the A_{made} sample and compared to C_{pulse} after 7 days of dynamic conditioning.

CTT was carried out on A_{static}, A_{pulse}, C_{static} and C_{pulse} and compared to A_{made}. Ring-shaped specimens ($n = 9$, axial length (L) of 4 ± 0.5 mm), cut from freshly extracted TDC–SFCs were tested using an ElectroForce Biodynamic® Test Instrument 5160 (Bose Corp., USA) using a 15 N load cell and *ad hoc* modified grips (two L-shaped fixtures of 1.3-mm-diameter) [29]. Tests were carried out in displacement control at a rate of 0.01 mm/s until complete failure [31,37]. The stress (ratio of force to resistance area of the tubular specimen (A_R)), was calculated using $A_R = 2t \times L$, where t is TDC–SFC thickness, from histological measurements. The ultimate circumferential tensile strength (UCTS) was calculated using the maximum stress value. The strain was calculated as a percentage of the initial specimen length. The apparent modulus was calculated from the slope of the linear phase of the stress–strain output.

An adaptation of Laplace's law for intraluminal pressure was used to estimate TDC–SFC burst pressure was calculated from UCTS as: $P_{burst} = (\text{UCTS} \times t)/R_0$, where t and R_0 represented the TDC–SFC thickness and intraluminal radius at atmospheric pressure, respectively [29,38–40].

Compliance was measured in order to evaluate the distension of A_{made} and C_{pulse}, in terms of unit of volume change per unit of pressure change ($n = 3$). A digital camera recorder measured TDC–SFC distension as a function of the external diameter, and a catheter pressure transducer simultaneously recorded the luminal pressure [29,40,41]. The images were post-processed with Adobe Photoshop to measure the external TDC–SFC diameter at each recorded pressure. Assuming an incompressible wall, the compliance of TDC–SFCs was calculated in the pressure range of 80–120 mmHg as follows $C = \{[(D_{120} - D_{80})/D_{80}]/\Delta P\} \times 10{,}000$, and expressed as % per 100 mmHg in accordance with an International Standard protocol [37], where D_{120} and D_{80} are the TDC–SFC external diameter measured at 120 and

80 mmHg, respectively, and ΔP is the variation of pressure during the measurement (*i.e.* 80–120 mmHg).

2.10. Statistical analysis

Data were analysed for statistical significance using a two-way ANOVA with a significance level = 0.05 and Tukey–Kramer and Holm–Bonferroni methods for means comparison (Origin Pro v.8 software, OriginLab, USA).

3. Results

3.1. MSC viability and distribution

MSC viability within C_{static} and C_{pulse} was assessed at day 7 in CD through CLSM of calcein-AM labelled and ethidium homodimer-1 positive cells (Fig. 1C). Maximum intensity z-stack projections were obtained from ring samples of TDC–SFC, where a uniform distribution of viable MSCs (with negligible presence of dead cells) was observed throughout the entire wall thickness of C_{static} and C_{pulse}. Moreover, MSCs were preferentially aligned within the different regions of the C_{pulse} wall when compared to those in C_{static}, which were randomly oriented. Optical microscopy of H&E stained histological sections confirmed the homogenous distribution of MSCs within the multilayered structure of C_{static} and C_{pulse} at day 7 in CD (Fig. 1C). Both CLSM and histology images indicated a greater distribution of MSCs within C_{pulse} compared to C_{static}.

3.2. MSC alignment

SEM and CLSM of F-actin stained cytoplasm were used to assess MSC alignment within C_{static}, $C_{laminar}$, and C_{pulse} at day 7 in CD (Fig. 2). SEM micrographs showed that MSCs displayed a random distribution within both the internal and external surfaces of C_{static}. This was confirmed by maximum intensity projections of z-stacks of intracellular stress fibres from inner and outer layers of 150-μm thicknesses. Laminar flow stimulation oriented MSCs along the fluid flow direction on the luminal TDC–SFC surface only, while there was no preferential distribution observed on the external surface. Under pulsatile flow, MSCs aligned at approximately 45° to the fluid flow direction on the internal surface and parallel to the circumferential strain (*i.e.* perpendicular to the fluid flow direction) on the external surface.

3.3. MSC chondrogenic differentiation

Chondrogenic differentiation of MSCs within C_{static}, $C_{laminar}$, and C_{pulse} in ND and CD was assessed at day 7 through the expression of Col2a1 and Agg using RT-qPCR (Fig. 3A). In order to evaluate the effect of laminar and pulsatile flow on the expression of chondrogenic markers under both ND and CD, the expression of the target genes within $C_{laminar}$, and C_{pulse} was normalized to that expressed within C_{static} under each culture condition. The expression of Col2a1 and Agg within $C_{laminar}$ was between 1- and 1.2-fold those measured within C_{static} in CD. In contrast, MSCs within C_{pulse} displayed a significant down-regulation of both Col2a1 and Agg in comparison to C_{static} and $C_{laminar}$ under ND and CD ($p < 0.05$).

Microscopic evaluation of Safranin-O stained histological sections of C_{static}, $C_{laminar}$, and C_{pulse} at day 7 in CD was used to investigate the distribution of glycosaminoglycans. There was a

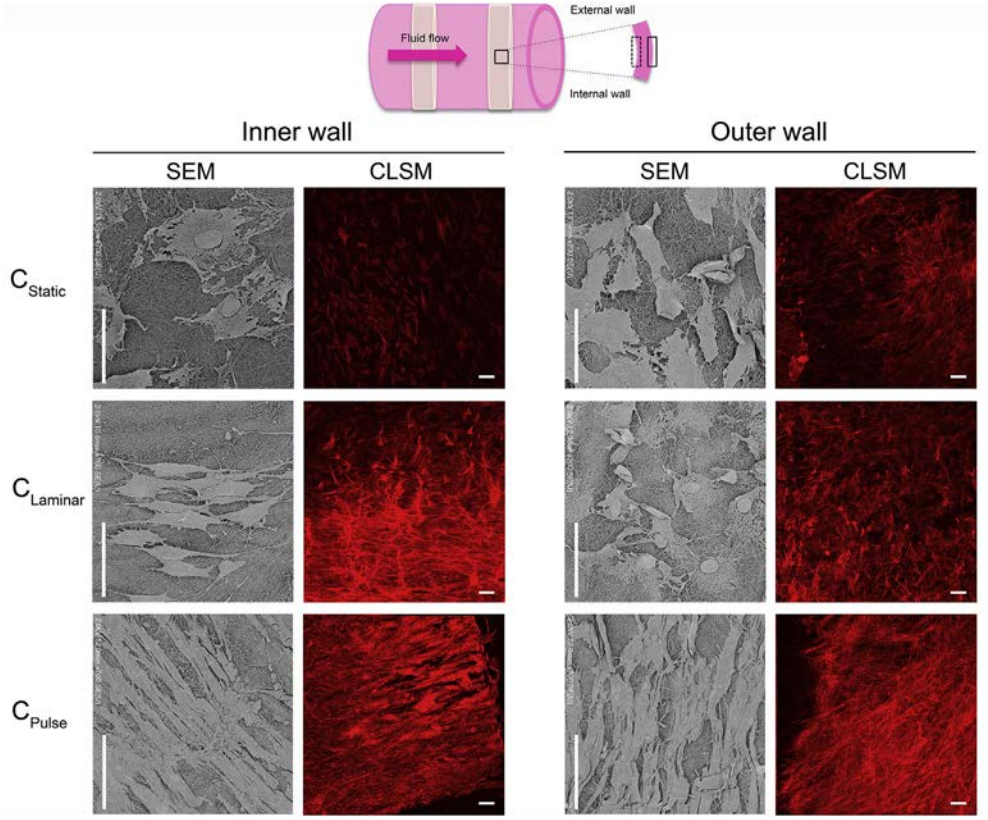

Fig. 2. MSC alignment. Left and right panels, SEM and CLSM (maximum intensity projections of F-actin staining from 150-μm z-stack) images of the inner and outer walls, respectively, of C_{static}, $C_{laminar}$ and C_{pulse} at day 7 in CD. MSCs were randomly oriented in C_{static}. In $C_{laminar}$, MSCs were aligned parallel to fluid flow direction within the internal wall and no preferential alignment was evident within the external wall. Under pulsatile flow, MSCs were aligned along the fluid flow direction within the inner wall, and orientated parallel to the circumferential strain imposed during the dynamic cycle within the outer wall. CLSM scale bar = 200 μm.

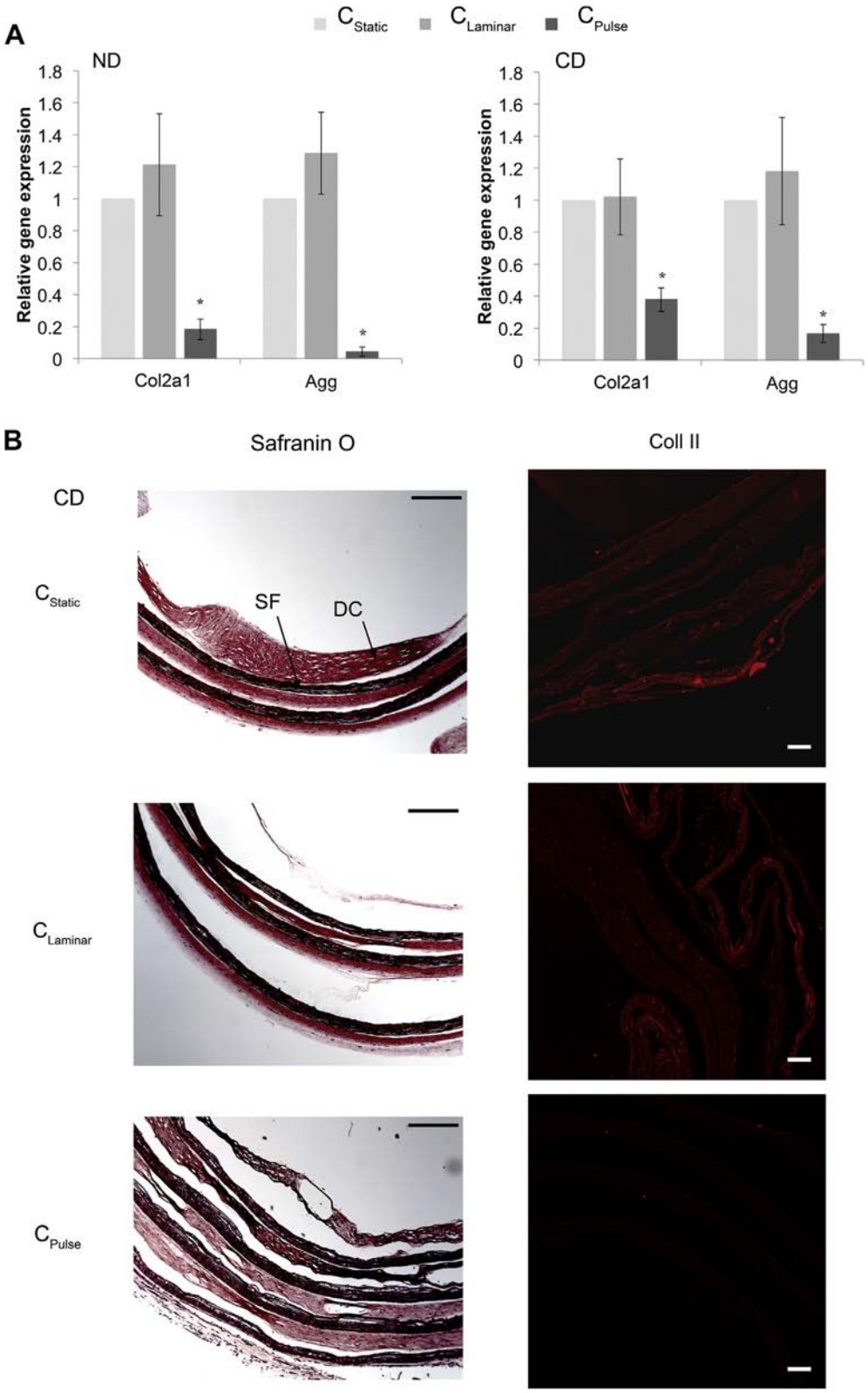

Fig. 3. Assessment of MSC chondrogenic differentiation. A. Changes in Col2a1, and Agg gene expression within $C_{laminar}$ and C_{pulse} relative to C_{static} at day 7 in ND and CD. In each culture condition, RNA expression of each gene was first normalized against the housekeeping gene (GAPDH) and then related to the normalized expression level of the target gene in C_{static}. Shear stress together with circumferential strain and circumferential strain alone significantly reduced the gene expression of both Col2a1 and Agg within TDC-SFC under both ND and CD ($p < 0.05$). *Significant effect of circumferential strain on gene expression ($p < 0.05$). B. Left and right panels, Safranin-O staining and collagen type II distribution, respectively, within histological sections of C_{static}, $C_{laminar}$ and C_{pulse} at day 7 in CD. Glycosaminoglycans distribution was confirmed to be present predominantly within C_{static} and $C_{laminar}$. Scale bar = 500 μm. CLSM maximum intensity analysis of histological sections displayed the presence of collagen type II production at different levels within the TDC–SFCs multilayered structure of C_{static}, and $C_{laminar}$. In comparison, the presence of collagen type II within C_{pulse} was negligible. Samples conditioned in ND did not show any positive staining for collagen type II (data not shown). Scale bar = 200 μm.

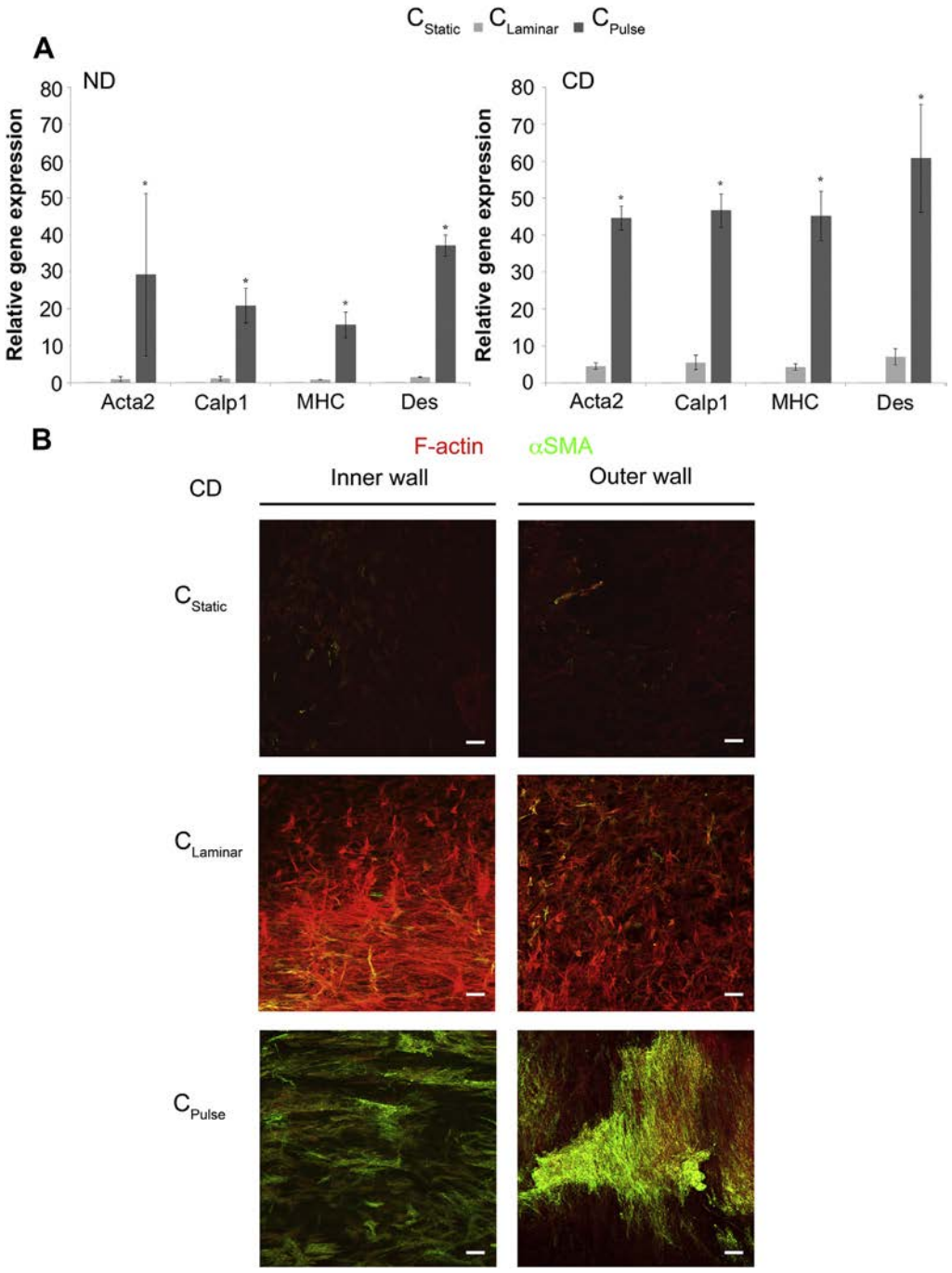

Fig. 4. Assessment of MSC contractile differentiation. A. Changes in Acta2, Calp1, MHC, and Des gene expression within $C_{laminar}$ and C_{pulse} relative to C_{static} at day 7 in ND and CD. In each culture condition, RNA expression of each gene was first normalized against the housekeeping gene (GAPDH) and then related to the normalized expression level of the target gene in C_{static}. Shear stress together with circumferential strain and circumferential strain alone significantly up-regulated the expression of the contractile markers of interest under both ND and CD ($p < 0.05$). *Significant effect of circumferential strain on gene expression ($p < 0.05$). B. Expression and distribution of αSMA protein within C_{static}, $C_{laminar}$, and C_{pulse} inner and outer walls by immunofluorescent staining. CLSM maximum intensity projections of F-actin (red) and αSMA (green) fibres obtained from 150-μm z-stack of TDC–SFC inner and outer walls. Few αSMA-positive stained cells were observed within C_{static}, and $C_{laminar}$. αSMA was strongly present within both the inner and outer walls of C_{pulse}, where MSCs were aligned parallel to the fluid flow and circumferential strain directions, respectively. Scale bar = 200 μm. (For interpretation of the references to colour in this figure legend, the reader is referred to the web version of this article.)

greater extent of positive red (in web version) stained area within C_{static}, and $C_{laminar}$ compared to C_{pulse} in CD (Fig. 3B), while no evidence of cartilage-like matrix were present in ND (data not shown). Moreover, red (in web version) stained regions were homogenously distributed within C_{static} and $C_{laminar}$, while randomly dispersed in localized internal regions of C_{pulse}.

CLSM investigation of anti-collagen type II antibody staining within histological sections of C_{static}, $C_{laminar}$, and C_{pulse} at day 7 in CD assessed collagen type II production (Fig. 3C). Maximum intensity projections of z-stacks of C_{static} and $C_{laminar}$ revealed the presence of collagen type II production at the different layers of TDC–SFCs. In contrast, the extent of collagen type II within C_{pulse} was negligible and mostly distributed at the interface of DC and SF.

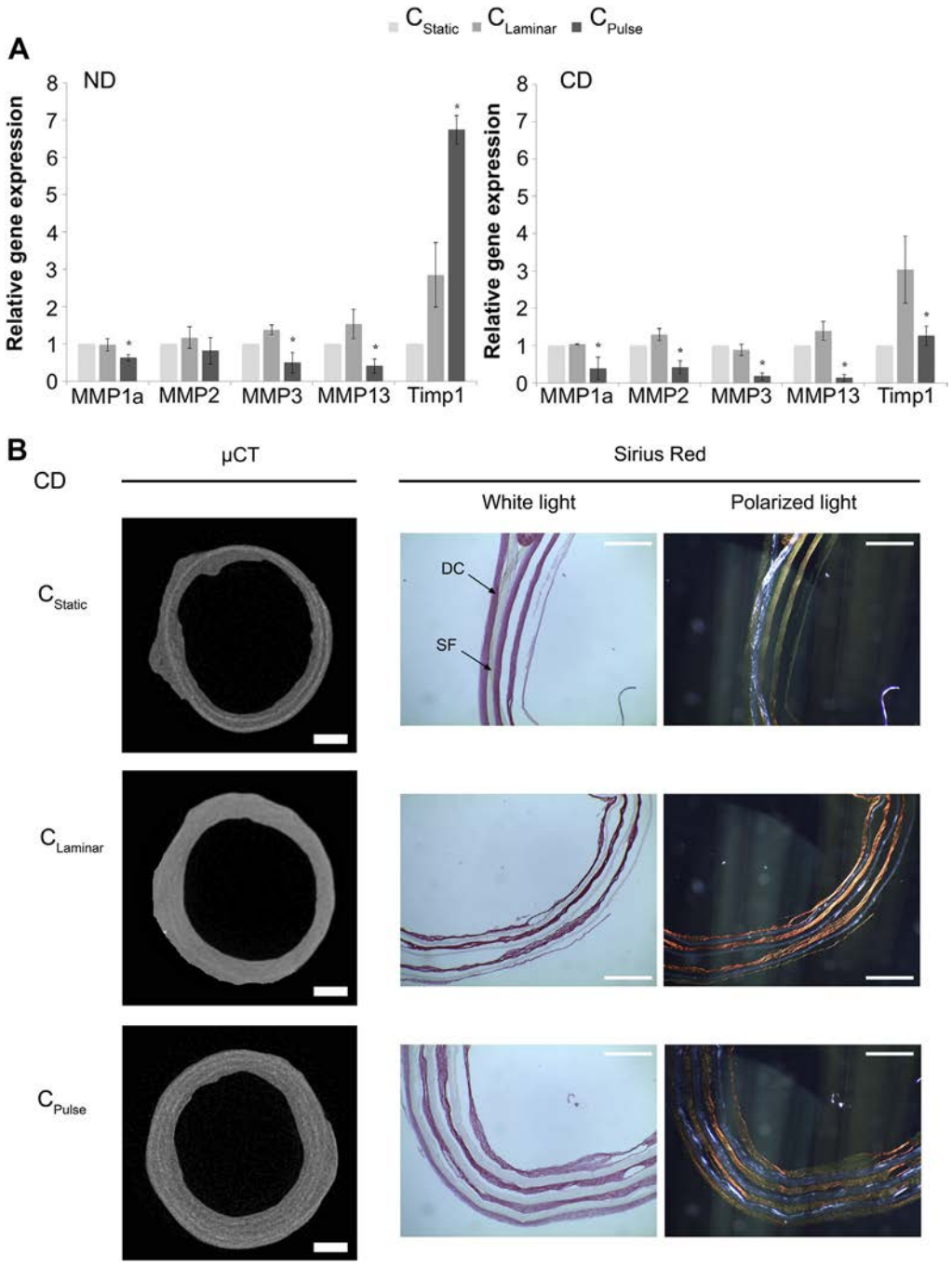

Fig. 5. Assessment of MSC-mediated remodelling. A. MMPs gene expression of MSCs. Changes in MMP1, MMP2, MMP3, MMP13, and Timp1 gene expression within $C_{laminar}$ and C_{pulse} relative to C_{static} at day 7 in ND and CD. In each culture condition, RNA expression of each gene was first normalized against the housekeeping gene (GAPDH) and then related to the normalized expression level of the target gene in C_{static}. In ND, MMPs expression (except for MMP2) was halved in C_{pulse} compared to C_{static}, while Timp1 was significantly up-regulated within C_{pulse} compared to $C_{laminar}$ and C_{static} ($p < 0.05$). In CD, there was a significant reduction in the expression of all MMPs in C_{pulse} compared to $C_{laminar}$, and Timp1 was down-regulated in C_{pulse} compared to $C_{laminar}$ ($p < 0.05$). *Significant effect of circumferential strain on gene expression ($p < 0.05$). B. TDC–SFC morphological properties. Two-dimensional microCT reconstructions of C_{static}, $C_{laminar}$, and C_{pulse} at day 7 in CD. The multilayered structure of TDC–SFC remained stable and cohesive over time under all conditions. $C_{laminar}$ and C_{static} displayed a more homogenous wall density in comparison to C_{pulse}, where the presence of SF layers (*) was still evident. Scale bar = 500 μm. SR stained histological sections displayed a greater extent in the birefringency in $C_{laminar}$ and C_{pulse} compared to C_{static}, reflecting an increase in the collagen fibrillar content. Scale bar = 500 μm.

3.4. MSC contractile differentiation

The potential of MSC differentiation into a contractile phenotype within $C_{laminar}$ and C_{pulse} in comparison to C_{static} under ND and CD was assessed at day 7. Measurement of the expression of Acta2, Calp1, MHC and Des via RT-qPCR indicated a significant up-regulation of all contractile markers in C_{pulse} compared to C_{static} and $C_{laminar}$ under both ND and CD ($p < 0.05$, Fig. 4A). The expression of MSC contractile markers in C_{pulse} was greater in CD compared to ND, in particular for Calp1 and MHC.

CLSM was used to investigate the detection and distribution of αSMA protein production within the inner and outer 150 μm-

thickness layers of C_{static}, $C_{laminar}$, and C_{pulse} in CD (Fig. 4B). C_{static} did not exhibit any presence of positive stained α-actin intracellular fibres. $C_{laminar}$ displayed few αSMA-positive stained cells within both the inner and outer layers. In contrast, C_{pulse} revealed a greater distribution of αSMA-positive stained MSCs, particularly within the outer layer where the cell population was greater when compared to the inner layer.

3.5. MMPs gene expression

The effect of dynamic stimulation on MSC-mediated remodelling of TDC–SFCs was assessed through RT-qPCR measurement of the expression of selected MMPs and MMP inhibitor at the transcription level within $C_{laminar}$ and C_{pulse} relative to C_{static} at day 7 under both ND and DC (Fig. 5A). The selected genes were all expressed within C_{static}, $C_{laminar}$ and C_{pulse} in both media. In particular, there was a significant down-regulation in the expression of MMP1a, MMP3, and MMP13 and up-regulation in Timp1 in C_{pulse} compared to C_{static} and $C_{laminar}$ ($p < 0.05$). Timp1 expression was up-regulated by more than 2-fold in $C_{laminar}$ in comparison to C_{static} in ND ($p < 0.05$). Analogously, there was a significant down-regulation in the expression of the selected MMPs and Timp1 in C_{pulse} compared to C_{static} and $C_{laminar}$ in CD ($p < 0.05$). Under laminar flow only MMP13 was expressed at a lower extent, along with Timp1 at a higher extent compared to C_{static} in both ND and CD.

3.6. TDC–SFC morphological properties

The effect of MSC-mediated remodelling on the morphology of TDC–SFCs was evaluated in C_{static}, $C_{laminar}$, and C_{pulse} at day 7 in CD (Fig. 5B). MicroCT was used to characterize the geometrical stability of the TDC–SFC multilayered structure, in particular at the interface between SF and DC. The analysis indicated the structural integrity of all TDC–SFCs and the absence of discontinuity or air pockets. The SF layers were evident within the walls of C_{pulse} and in certain regions of C_{static}, while $C_{laminar}$ demonstrated a more compact and homogenous density in the wall. In addition, C_{pulse} wall thickness (464 ± 49 μm) was significantly greater compared to C_{static} (288 ± 20 μm), and $C_{laminar}$ (341 ± 64 μm) ($p < 0.05$).

SR stained histological sections were analysed under white and polarized light microscopy to characterize fibrillar collagen organization. The birefringency of the collagen structure was greater within $C_{laminar}$ and C_{pulse} in comparison to C_{static}, reflecting a greater collagen fibrillar content.

3.7. TDC–SFC mechanical properties

Representative CTT stress–strain curves of A_{made}, A_{static}, A_{pulse}, C_{static}, and C_{pulse} displayed the characteristic behaviour of soft tissues. Three distinct regions can be identified: toe, which displayed a non-linear response at low strain; linear, where the apparent modulus was calculated; and failure, where the UCTS was calculated (Fig. 6A). The apparent modulus was not affected by culturing ($p > 0.05$, Fig. 6B). In addition, there was no statistical significant difference in UCTS values for all TDC–SFCs in comparison to A_{made} ($p > 0.05$) (Fig. 6C) and that of C_{pulse} was significantly greater compared to A_{static} and A_{pulse} ($p < 0.05$). The estimated TDC–SFC burst pressure values under all stimuli were not statistically different to A_{made} ($p > 0.05$) (Fig. 6D). However, the estimated burst pressure of C_{pulse} was significantly higher than those of A_{static} and A_{pulse} ($p < 0.05$). In addition, the compliance of C_{pulse} was lower compared to A_{made} ($p < 0.05$, Fig. 6E).

4. Discussion

Native tissues respond to a large variety of dynamic environmental cues, which in concert direct cell growth, function, and phenotype [42]. These cues can be biochemical, matrix-dependent, or mechanical. Growth factors and extracellular matrix (ECM) macromolecules are fundamental in maintaining tissue architecture and modulating cellular functions, via integrin receptors. At the same time, mechanical cues are transferred by the matrix to cells through integrin-mediated signalling, which connect the external environment to intracellular structures. Therefore, tissue engineering constructs should sustain cell growth and organization, and transfer physiologically equivalent mechanical stimuli; factors that are strongly influenced by the matrix morphological and mechanical properties [43]. The TDC–SFC developed in this study, with mechanical and morphological properties similar to native trachea [44], underscored the central role of 3D matrix in the delivery of mechanical stimuli over chemical factors, by providing an *in vitro* niche to control MSC fate and matrix-mediated remodelling.

The ability to direct seeded MSC differentiation through the combination of a meso-structured natural polymer-based matrix and the delivery physiologically relevant dynamic mechanical forces allows for the engineering of numerous complex tissues populated by multiple cell types. This process is more controllable than cell-based technologies and negates the use of cadaver- or synthetic material-derived tissue substitutes [3,7,45,46]. TDC–SFCs combined the biological features of a DC matrix with cartilage ring-like electrospun SF insertions, thus mimicking the airway tract physiological architecture. In addition, DC-based tubular constructs can be easily produced in less than an hour, with a high level of control on collagen fibrillar and cell density efficiency, growth and viability [29]; and can be effectively used to study cellular responses to physiologically relevant dynamic conditioning [31].

MSC viability and homogenous distribution throughout the entire wall was confirmed in C_{static} and C_{pulse} at day 7 in CD, where the application of pulsatile flow clearly stimulated cell growth in comparison to static culture. Fluid flow most likely altered the transport of oxygen and nutrients within the construct. Diffusion would dominate mass transport within C_{static}, while under pulsatile flow the convective contribution may increase such transport, resulting in an increase in MSC growth, as previously quantified [31,47].

It is well known that mechanical stimulation plays an important role in MSC differentiation toward chondrogenic, osteogenic, and contractile lineages [18,23,48,49]. In particular, many studies focused on the effect of dynamic stimulation on MSC behaviour are mostly over a week period, as mechanical cues play a crucial role in their differentiation state and significant effects have been shown as early as day 3 in culture [50–54]. Chondrogenic differentiation can be induced via cyclic dynamic compression [49], while MSC contractile phenotype can be stimulated through cyclic mechanical strain [55]. However, it would be beneficial to identify the effect of chemical and mechanical cues in selectively modulating MSC fate in order to mimic the complexity of native tissues populated by various cell types. The application of mechanical stimulation preferentially aligns MSCs on either two-dimensional or within three-dimensional substrates. MSCs have been shown to align only in the direction perpendicular to the applied strain (parallel to the flow, in case of tubular geometry) [19,21,48,55,56]. This is in contrast to the native orientation of smooth muscle cells subjected to similar stimuli, *in vivo*, which align parallel to the strain (*i.e.* circumferential direction) or in a helical pattern [18]. In addition, the extent of cyclic strain influences MSC alignment in order to prevent cellular damage under strains greater than 5%

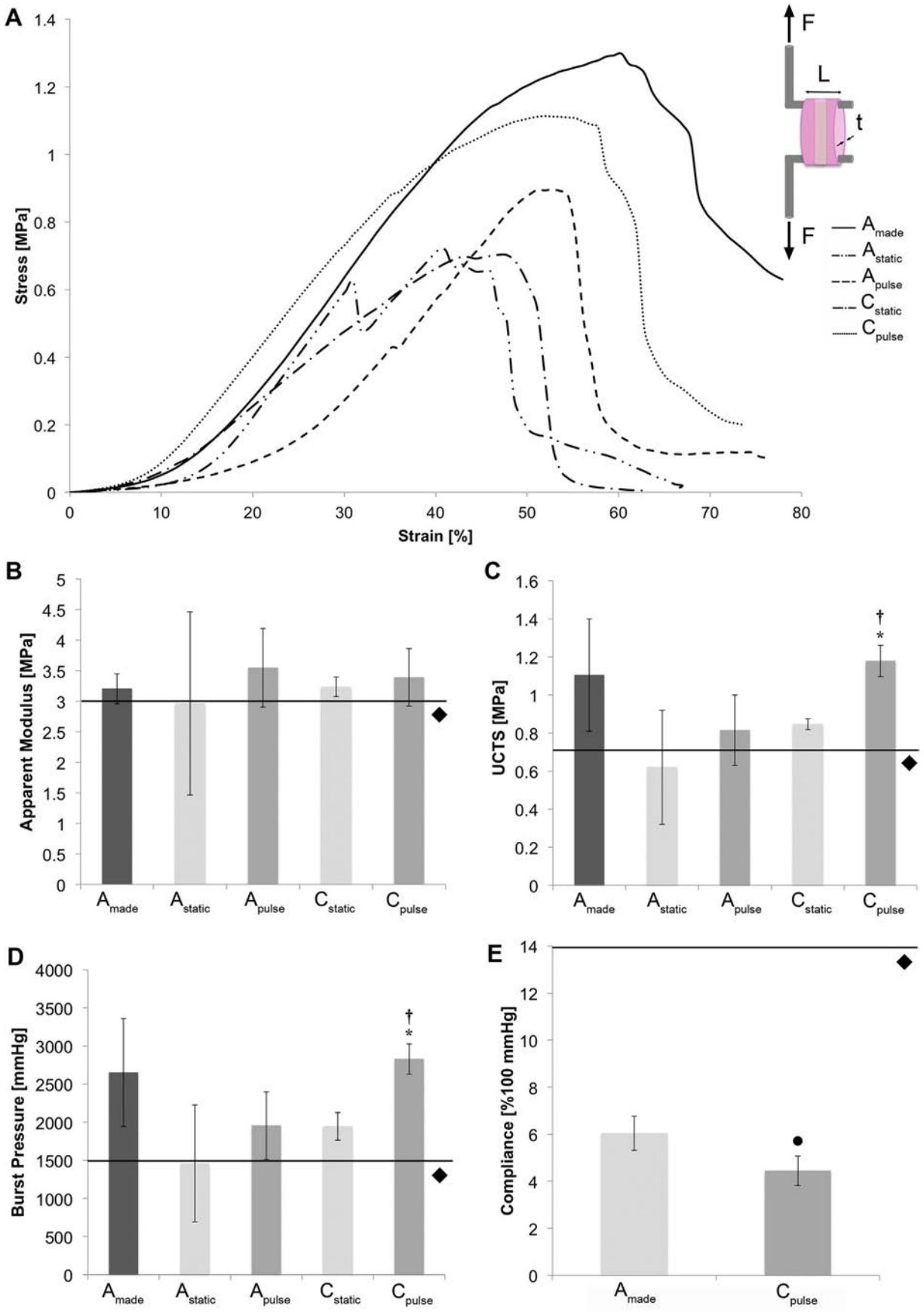

Fig. 6. TDC–SFC mechanical properties. A. Representative stress–strain curves in the circumferential direction for A_{made}, A_{static}, A_{pulse}, C_{static} and C_{pulse} in CD. B. Apparent modulus. C. UCTS. D. Burst pressure, estimated in accordance to Laplace relationship, as a function of UCTS, TDC–SFC wall thickness and unpressurized radius. E. The value of compliance for C_{pulse} in comparison to A_{made} was calculated between 80 and 120 mmHg. The mechanical properties are compared with previously reported TDCC values based on bovine dermis collagen derivation (υ) [28]. † Significant effect of MSC-mediated remodelling combined with pulsatile flow on TDC–SFC mechanical properties; *significant effect of MSC-mediated remodelling on TDC–SFC mechanical properties. • Significant effect of MSC-mediated remodelling combined with pulsatile flow on TDC-SFC compliance. ($p < 0.05$).

[19,21,55,56]. In this study, MSCs seeded within the luminal layers of both $C_{laminar}$ and C_{pulse} and cultured in CD, aligned parallel to the direction of fluid flow, as a consequence of being directly exposed to physiological shear stress [31]. In contrast, the outer layers and surfaces of C_{pulse} displayed an orientation parallel to the circumferential cyclic strain (<5%); compatible with physiological conditions. In contrast, and as previously reported [31], $C_{laminar}$ did not exhibit a similar effect; where MSCs were randomly distributed within the outer layer. The effect of shear stress on luminal epithelium organization has been shown to dominate over radial distension [44], while the lack of cell alignment within the outer layer of $C_{laminar}$ demonstrated the dominance of circumferential strain over shear stress at increased distances from the lumen within C_{pulse}. In comparison, MSCs seeded within C_{static} were randomly oriented on both the internal and external walls.

The significant up-regulation of selected contractile markers, including Acta2, Calp1, MHC, and Des, and the distribution of αSMA in CD under pulsatile flow in comparison to both C_{static} and $C_{laminar}$ suggests that the application of a cyclic strain together with cyclic shear stress overcomes the effect of growth factors and is a more powerful tool than shear stress alone in directing MSC fate [19]. In addition, the extent of contractile marker up-regulation within C_{pulse} in comparison to C_{static} and $C_{laminar}$ was greater in CD compared to ND. Indeed, TGF-beta, one of the chondrogenic supplements used in this study, is also implicated in the function of MSCs in blood vessel maturation [57]. Therefore, the effect of cyclic circumferential strain on MSC phenotype was amplified by the influence of TGF-beta, as a synergistic biochemical factor. As a consequence, the chondrogenic potential of MSCs after 7 days in CD was significantly enhanced under static and laminar culture conditions, as demonstrated by the up-regulation of Col2a1 and Agg gene expression, greater extent of cartilage-like matrix stained with Safranin-O, and increased Coll II production. Moreover, uniaxial strain has been shown to significantly decrease MSC chondrogenic differentiation and cartilage matrix protein production, suggesting that cyclic stress reduces the phenotype of compression-bearing tissues in favour of other lineages (*i.e.* muscle) [18]. These findings underscore the central role of a native-like 3D matrix in the delivery of mechanical stimuli over chemical factors in modulating MSC phenotype. A balance between MSC contractile and chondrogenic states may be achieved through a combination of laminar and pulsatile flow regimes to engineer the airway native cell–tissue composition.

The regulation of matrix remodelling is balanced at the transcription level by MMPs and their endogenous inhibitors, Timps [58]. In particular, collagen remodelling comprises a complex set of events where, in analogy to native ECM, is continuously digested by synchronous proteolytic degradation (activated by MMPs) and reassembled by cells (through endogenous collagen production), eventually resulting in morphological and structural changes [59]. Generally, the gene expression of the selected MMPs was down-regulated within C_{pulse} in comparison to C_{static} and $C_{laminar}$, particularly for MMP1 and MMP13, which are involved in type I collagen remodelling [60,61], and MMP3, the major substrate of which are the proteoglycans [60]. The extent of MMP down-regulation upon cyclic circumferential strain, in comparison to C_{static} and $C_{laminar}$, was greater in CD than in ND. Uniaxial cyclic strain has been previously shown to induce a decrease in MMP1 activity, and promoting the assembly of collagen fibrils [18]. MicroCT analysis indicated that the multilayered structure of C_{static} and $C_{laminar}$ appeared to be more compact and remodelled compared to C_{pulse}, which displayed a greater wall thickness and clear distinctions between DC and SF insertions. Furthermore, the extent of MSC-mediated remodelling and ECM production was evaluated through SR staining of organized collagen fibrils. Collagen fibrils birefringency was scarcely present within C_{static}, in comparison to $C_{laminar}$ and C_{pulse}, suggesting that the production of endogenous ECM was not mainly based on fibrillar collagen, probably in favour of proteoglycan deposition, as also demonstrated by positive red Safranin-O staining within C_{static}, and up-regulation in the expression of Col2a1 and Agg.

The effect of MSC-mediated activity on TDC–SFC structure in response to dynamic stimulation in CD was assessed in terms of construct mechanical properties. It has been previously reported that cyclic loading significantly increased collagen gel-based construct mechanical strength [31,62]. In the case of TDC–SFC, the application of dynamic stimulation on acellular constructs did not affect mechanical properties. The increased fibrillar aggregation, resulting from the cyclic loading [62], which increased the dense collagen construct mechanical properties, may be negligible as a consequence of the overriding effect of the SF insertions. In addition, the increase in UCTS of C_{pulse} in comparison to the other samples, except for A_{made}, may be due to the positive effect of MSC activity under pulsatile flow. In comparison to tubular dense collagen construct (TDCC) alone, produced from the same bovine collagen derivation, TDC–SFC displayed greater UCTS for A_{made}, C_{static}, and C_{pulse}, demonstrating the reinforcing role of the SF insertions [29]. The estimated burst pressure of A_{made}, C_{static}, and C_{pulse} was higher than that of TDCC. Furthermore, TDC–SFC mechanical properties were found to be in the same order of magnitude of those measured for human tracheal cartilage rings [44], thus overcoming the general limitations of natural polymer-based scaffolds. In addition, the compliance of C_{pulse} was significantly lower compared to those of A_{made} and TDCC, suggesting an increase in the construct rigidity, and therefore, structural stability.

5. Conclusions

TDC–SFC, which mimicked the native airway tract architecture, maintained seeded MSC growth and distribution. Their ability to transfer physiologically relevant mechanical stimuli to seeded MSCs resulted in native-like cell orientation within the tubular tissue models, when subjected to pulsatile flow-induced cyclic circumferential strain, and induced MSC contractile phenotype expression, regardless of the chemical factors supplied during *in vitro* culture. On the other hand, static culture and laminar flow enhanced MSC chondrogenic differentiation. In addition, the effects of MSC-mediated activity upon pulsatile flow resulted in a reduction in matrix remodelling and increased construct stability.

Acknowledgements

This work was supported by the Canadian Natural Sciences and Engineering Research Council, the Canadian Foundation for Innovation: Leaders Opportunity Funds, Quebec MESRST, and McGill University Faculty of Engineering Gerald Hatch Faculty Fellowship.

References

[1] Griffith LG, Naughton G. Tissue engineering – current challenges and expanding opportunities. Science 2002;295:1009–14.
[2] Griffith LG, Swartz MA. Capturing complex 3D tissue physiology in vitro. Nat Rev Mol Cell Biol 2006;7:211–24.
[3] Ott L, Weatherly R, Detamore M. Overview of tracheal tissue engineering: clinical need drives the laboratory approach. Ann Biomed Eng 2011;39:2091–113.
[4] Kamm RD. Airway wall mechanics. Annu Rev Biomed Eng 1999;1:47–72.
[5] Vacanti CA, Paige KT, Kim WS, Sakata J, Upton J, Vacanti JP. Experimental tracheal replacement using tissue-engineered cartilage. J Pediatr Surg 1994;29:201–5.
[6] Kojima K, Bonassar LJ, Roy AK, Mizuno H, Cortiella J, Vacanti CA. A composite tissue-engineered trachea using sheep nasal chondrocyte and epithelial cells. FASEB J 2003;17:823–8.

[7] Kojima K, Bonassar LJ, Roy AK, Vacanti CA, Cortiella J. Autologous tissue-engineered trachea with sheep nasal chondrocytes. J Thorac Cardiovasc Surg 2002;123:1177–84.
[8] Dunham B, Flint P, Singhal S, Visage CL, Leong K. Tracheal tissue engineering. In: Bronzino JD, editor. The biomedical engineering handbook. Taylor & Francis Group; 2006.
[9] Komura M, Komura H, Kanamori Y, Tanaka Y, Suzuki K, Sugiyama M, et al. An animal model study for tissue-engineered trachea fabricated from a biodegradable scaffold using chondrocytes to augment repair of tracheal stenosis. J Pediatr Surg 2008;43:2141–6.
[10] Omori K, Nakamura T, Kanemaru S, Asato R, Yamashita M, Tanaka S, et al. Regenerative medicine of the trachea: the first human case. Ann Otol Rhinol Laryngol 2005;114:429–33.
[11] Lin CH, Su JM, Hsu SH. Evaluation of type II collagen scaffolds reinforced by poly(epsilon-caprolactone) as tissue-engineered trachea. Tissue Eng Part C Methods 2008;14:69–77.
[12] Lin CH, Hsu SH, Huang CE, Cheng WT, Su JM. A scaffold-bioreactor system for a tissue-engineered trachea. Biomaterials 2009;30:4117–26.
[13] Henderson JH, Welter JF, Mansour JM, Niyibizi C, Caplan AI, Dennis JE. Cartilage tissue engineering for laryngotracheal reconstruction: comparison of chondrocytes from three anatomic locations in the rabbit. Tissue Eng 2007;13:843–53.
[14] Ni Y, Zhao X, Zhou L, Shao Z, Yan W, Chen X, et al. Radiologic and histologic characterization of silk fibroin as scaffold coating for rabbit tracheal defect repair. Otolaryng Head Neck 2008;139:256–61.
[15] Caplan AI. Adult mesenchymal stem cells for tissue engineering versus regenerative medicine. J Cell Physiol 2007;213:341–7.
[16] Pittenger MF, Mackay AM, Beck SC, Jaiswal RK, Douglas R, Mosca JD, et al. Multilineage potential of adult human mesenchymal stem cells. Science 1999;284:143–7.
[17] Engler AJ, Sen S, Sweeney HL, Discher DE. Matrix elasticity directs stem cell lineage specification. Cell 2006;126:677–89.
[18] Kurpinski K, Chu J, Hashi C, Li S. Anisotropic mechanosensing by mesenchymal stem cells. Proc Natl Acad Sci U S A 2006;103:16095–100.
[19] Huang Y, Zheng L, Gong X, Jia X, Song W, Liu M, et al. Effect of cyclic strain on cardiomyogenic differentiation of rat bone marrow derived mesenchymal stem cells. PloS One 2012;7:e34960.
[20] Riddle RC, Taylor AF, Genetos DC, Donahue HJ. MAP kinase and calcium signaling mediate fluid flow-induced human mesenchymal stem cell proliferation. Am J Physiol Cell Physiol 2006;290:C776–84.
[21] Hamilton DW, Maul TM, Vorp DA. Characterization of the response of bone marrow-derived progenitor cells to cyclic strain: implications for vascular tissue-engineering applications. Tissue Eng 2004;10:361–9.
[22] Mouw JK, Connelly JT, Wilson CG, Michael KE, Levenston ME. Dynamic compression regulates the expression and synthesis of chondrocyte-specific matrix molecules in bone marrow stromal cells. Stem Cells 2007;25:655–63.
[23] Sharp LA, Lee YW, Goldstein AS. Effect of low-frequency pulsatile flow on expression of osteoblastic genes by bone marrow stromal cells. Ann Biomed Eng 2009;37:445–53.
[24] Moreau JE, Bramono DS, Horan RL, Kaplan DL, Altman GH. Sequential biochemical and mechanical stimulation in the development of tissue-engineered ligaments. Tissue Eng Part A 2008;14:1161–72.
[25] Arai T, Freddi G, Innocenti R, Tsukada M. Biodegradation of *Bombyx mori* silk fibroin fibers and films. J Appl Polym Sci 2004;91:2383–90.
[26] Ghezzi CE, Marelli B, Muja N, Hirota N, Martin JG, Barralet JE, et al. Mesenchymal stem cell-seeded multilayered dense collagen-silk fibroin hybrid for tissue engineering applications. Biotechnol J 2011;6:1198–207.
[27] Alessandrino A, Marelli B, Arosio C, Fare S, Tanzi MC, Freddi G. Electrospun silk fibroin mats for tissue engineering. Eng Life Sci 2008;8:219–25.
[28] Wilson D, Valluzzi R, Kaplan D. Conformational transitions in model silk peptides. Biophys J 2000;78:2690–701.
[29] Ghezzi CE, Marelli B, Muja N, Nazhat SN. Immediate production of a tubular dense collagen construct with bioinspired mechanical properties. Acta Biomater 2012;8:1813–25.
[30] Rockwood DN, Preda RC, Yucel T, Wang XQ, Lovett ML, Kaplan DL. Materials fabrication from *Bombyx mori* silk fibroin. Nat Protoc 2011;6:1612–31.
[31] Ghezzi CE, Risse P-A, Marelli B, Muja N, Barralet JE, Martin JG, et al. An airway smooth muscle cell niche under physiological pulsatile flow culture using a tubular dense collagen construct. Biomaterials 2013;34:1954–66.
[32] Fung YC. Biomechanics: mechanical properties of living tissues. 2nd ed. New York: Springer-Verlag; 1993.
[33] Favre E, Thaler T. An engineering analysis of rotating sieves for hybridoma cell retention ins stirred tank bioreactors. Cytotechnology 1992;9:11–9.
[34] Sidhaye VK, Schweitzer KS, Caterina MJ, Shimoda L, King LS. Shear stress regulates aquaporin-5 and airway epithelial barrier function. Proc Natl Acad Sci U S A 2008;105:3345–50.
[35] Livak KJ, Schmittgen TD. Analysis of relative gene expression data using real-time quantitative PCR and the 2deltadeltaCt method. Methods 2001;25:402–8.
[36] Junqueira L, Bignolas G, Brentani R. Picrosirius staining plus polarization microscopy, a specific method for collagen detection in tissue sections. Histochem J 1979;11:447–55.
[37] (E) Cardiovascular implants – tubular vascular prostheses. International Organization for Standardization.ISO 7198; 1998.
[38] Lai ES, Anderson CM, Fuller GG. Designing a tubular matrix of oriented collagen fibrils for tissue engineering. Acta Biomater 2011;7:2448–56.
[39] Nieponice A, Soletti L, Guan J, Deasy BM, Huard J, Wagner WR, et al. Development of a tissue-engineered vascular graft combining a biodegradable scaffold, muscle-derived stem cells and a rotational vacuum seeding technique. Biomaterials 2008;29:825–33.
[40] Konig G, McAllister TN, Dusserre N, Garrido SA, Iyican C, Marini A, et al. Mechanical properties of completely autologous human tissue engineered blood vessels compared to human saphenous vein and mammary artery. Biomaterials 2009;30:1542–50.
[41] Dahl SLM, Koh J, Prabhakar V, Niklason LE. Decellularized native and engineered arterial scaffolds for transplantation. Cell Transpl 2003;12:659–66.
[42] Stegemann JP, Hong H, Nerem RM. Mechanical, biochemical, and extracellular matrix effects on vascular smooth muscle cell phenotype. J Appl Phys 2005;98:2321–7.
[43] Wilson E, Sudhir K, Ives HE. Mechanical strain of rat vascular smooth-muscle cells is sensed by specific extracellular matrix/integrin interactions. J Clin Invest 1995;96:2364–72.
[44] Rains JK, Bert JL, Roberts CR, Pare PD. Mechanical-properties of human tracheal cartilage. J Appl Phys 1992;72:219–25.
[45] Macchiarini P, Jungebluth P, Go T, Asnaghi MA, Rees LE, Cogan TA, et al. Clinical transplantation of a tissue-engineered airway. Lancet 2008;372:2023–30.
[46] Baiguera S, Del Gaudio C, Jaus MO, Polizzi L, Gonfiotti A, Comin CE, et al. Long-term changes to in vitro preserved bioengineered human trachea and their implications for decellularized tissues. Biomaterials 2012;33:3662–72.
[47] Khan OF, Chamberlain MD, Sefton MV. Toward an in vitro vasculature: differentiation of mesenchymal stromal cells within an endothelial cell-seeded modular construct in a microfluidic flow chamber. Tissue Eng Part A 2012;18:744–56.
[48] O'Cearbhaill ED, Punchard MA, Murphy M, Barry FP, McHugh PE, Barron V. Response of mesenchymal stem cells to the biomechanical environment of the endothelium on a flexible tubular silicone substrate. Biomaterials 2008;29:1610–9.
[49] Thorpe SD, Buckley CT, Vinardell T, O'Brien FJ, Campbell VA, Kelly DJ. The response of bone marrow-derived mesenchymal stem cells to dynamic compression following TGF-beta 3 induced chondrogenic differentiation. Ann Biomed Eng 2010;38:2896–909.
[50] Park SH, Sim WY, Min BH, Yang SS, Khademhosseini A, Kaplan DL. Chip-based comparison of the osteogenesis of human bone marrow- and adipose tissue-derived mesenchymal stem cells under mechanical stimulation. PloS One 2012;7:e46689.
[51] Tong Z, Duncan RL, Jia X. Modulating the behaviors of mesenchymal stem cells via the combination of high-frequency vibratory stimulations and fibrous scaffolds. Tissue Eng Part A 2013;19:1862–78.
[52] Teh TK, Toh SL, Goh JC. Aligned fibrous scaffolds for enhanced mechanoresponse and tenogenesis of mesenchymal stem cells. Tissue Eng Part A 2013;19:1360–72.
[53] Mayer M, Rabindranath R, Borner J, Horner E, Bentz A, Salgado J, et al. Ultrasoft PDMS-based magnetoactive elastomers as dynamic cell culture substrata. PloS One 2013;8:e76196.
[54] Pedersen TO, Blois AL, Xue Y, Xing Z, Sun Y, Finne-Wistrand A, et al. Mesenchymal stem cells induce endothelial cell quiescence and promote capillary formation. Curr Stem Cell Res Ther 2014;5:23.
[55] Park JS, Chu JSF, Cheng C, Chen F, Chen D, Li S. Differential effects of equiaxial and uniaxial strain on mesenchymal stem cells. Biotechnol Bioeng 2004;88:359–68.
[56] Nieponice A, Maul TM, Cumer JM, Soletti L, Vorp DA. Mechanical stimulation induces morphological and phenotypic changes in bone marrow-derived progenitor cells within a three-dimensional fibrin matrix. J Biomed Mater Res A 2007;81A:523–30.
[57] Frontini MJ, Nong Z, Gros R, Drangova M, O'Neil C, Rahman MN, et al. Fibroblast growth factor 9 delivery during angiogenesis produces durable, vasoresponsive microvessels wrapped by smooth muscle cells. Nat Biotechnol 2011;29:421–7.
[58] Birkedal-Hansen H, Moore WGI, Bodden MK, Windsor LJ, Birkedal-Hansen B, DeCarlo A, et al. Matrix metalloproteinases: a review. Crit Rev Oral Biol Med 1993;4:197–250.
[59] Sengupta S, Park S-H, Seok GE, Patel A, Numata K, Lu C-L, et al. Quantifying osteogenic cell degradation of silk biomaterials. Biomacromolecules 2010;11:3592–9.
[60] Daniels JT, Cambrey AD, Occleston NL, Garrett Q, Tarnuzzer RW, Schultz GS, et al. Matrix metalloproteinase inhibition modulates fibroblast-mediated matrix contraction and collagen production in vitro. Invest Ophthalmol Vis Sci 2003;44:1104–10.
[61] Visse R, Nagase H. Matrix metalloproteinases and tissue inhibitors of metalloproteinases. Circ Res 2003;92:827–39.
[62] Cheema U, Chuo CB, Sarathchandra P, Nazhat SN, Brown RA. Engineering functional collagen scaffolds: cyclical loading increases material strength and fibril aggregation. Adv Funct Mater 2007;17:2426–31.